

AMINO-SUBSTITUTED PORPHYRINS AT THE BORDER OF HYBRID MATERIALS GENERATION AND PLATINUM NANOPARTICLES DETECTION

DIANA ANGHEL^a, MIHAELA BIRDEANU^b, ANCA LASCU^a,
CAMELIA EPURAN^a, EUGENIA FAGADAR-COSMA^{a*}

ABSTRACT. Two amino substituted porphyrins, namely: 5,10,15,20-tetrakis(4-aminophenyl)porphyrin (TAPP) and 5,10,15,20-tetrapyridyl-21H,23H-porphine (TPyP) have been used for complexation reaction of platinum nanoparticles (PtNPs) with the main purpose to recover or detect them from diluted leaching solutions, after transformation in colloidal solutions. The complexation reactions were monitored by UV-vis spectroscopy and revealed that both porphyrins have the capacity to complex PtNPs in different detection domains ranging from 2.776 to 40.457 x 10⁻⁶ M in the case of TAPP, and in a larger range of 8.07 x 10⁻⁶ – 7.03 x 10⁻⁵ M in the case of TPyP. Excellent correlation coefficients of 99.35 % and 99.57 % respectively have been obtained in each case. During complexation a nanomaterial based on TAPP and a micromaterial composed from TPyP both having as second partner PtNPs were obtained and thoroughly characterized by atomic force microscopy (AFM). The aggregation phenomena that occurred for each amino-porphyrin in DMF, in their acidified solutions and in their hybrid materials, revealed that the TAPP-PtNPs hybrid is a nanomaterial, based on triangular prisms aggregates of acidulated TAPP, and the TPyP-PtNPs hybrid is a micromaterial that is based on pyramidal shaped aggregated from the acidulated solution of TPyP.

Keywords: amino-substituted porphyrins, PtNPs, Pt-NPs detection, UV-vis spectroscopy, AFM characterization

^a Institute of Chemistry "Coriolan Dragulescu", Mihai Viteazu Ave. 24, 300223 - Timisoara, Romania

^b National Institute for Research and Development in Electrochemistry and Condensed Matter, P. Andronescu Street 1, 300224- Timisoara, Romania

* Corresponding author: efagadar@yahoo.com

INTRODUCTION

In the last few years, the chemistry of porphyrins and metalloporphyrins has received increased interest. The conjugated electron system of the tetrapyrrolic macrocycle leads to unique optical properties used in a large range of applications in: medicine (for photodynamic therapies) [1], analytical chemistry (molecular recognition) [2], catalysis (mediators in electrochemistry and in organic synthesis) [3, 4], artificial photosynthesis [5] and as photosensitizers for organic solar cells [6, 7, 8] and in automotive industry [9].

This interest also covers the field of platinum nanoparticles due to the many uses of nanosized sensors [10, 11], catalysts [12] and drugs [13]. Platinum colloidal particles can be obtained by using different types of reduction agents [14], such as: trisodium citrate [15], aminodextrans [16], NaBH₄, is used to initiate the reaction, forming small particles [17].

For instance, the synthesis in ethylene glycol applying UV-induced reduction offers both a higher stability and a lower size of the particles [18, 19]. The stabilization of colloidal particles is possible by encapsulation in polymers, such as: polyvinyl alcohol (PVA), polyvinylpyrrolidone (PVP), polyacrylates, polyacrylamides, poly(ethylene glycol) (PEG) or by using surfactant agents, such as: cetyltrimethyl ammonium bromide (CTAB) that allow the formation of micelles [20, 21]. When stabilized with biocompatible polymers, like PVP, platinum nanoparticles have a beneficial effect upon the blood fluidity, under oxidative stress conditions [22].

The protective layer of the metal nanoparticles can be done also by covering them with different dyes that might improve the catalytic or sensitive properties of the colloids [23, 24]. Porphyrin molecules can perform this task with multiple benefits. For example, nanocomposites based on *meso*-tetrakis(*p*-sulfonatophenyl)porphyrin and PtNPs are photocatalytically active for water reduction to produce hydrogen under UV-vis irradiation [25]. An efficient hydrogen reduction photocatalyst was obtained from PtNPs and Zn(II)-protoporphyrin IX as photosensitizer [26]. Photosensitizer nanocomposites, formed from platinum nanoparticles functionalized with multibranching-porphyrins are reported to generate donor-bridge-acceptor conjugates, thus facilitating the electron transfer [27].

The interest in recovery or detection of platinum is nowadays continuously increasing, as the natural resources are limited and the consumption as catalyst in various chemical reactions, especially in automotive industry, is very large. The best performance of 600mg/g recovery imply biosorption of platinum using cellulose nano- fibers and nanocrystals modified with polyethylene imine [28]. Biomass materials [29], zeolites bearing hydrazine groups [30] or hybrids of oxalic acid [31] gave lower recovery performances of maximum 150 mg/g.

Other reported methods used in the last five years for platinum recovery are microwave-assisted with cloud point extraction [32], complexation [33-34] and ion exchange techniques, all from leaching solutions [35-37].

As most methods for the recovery of platinum that are economically feasible and environmentally friendly rely on adsorption phenomena, the purpose of our study was to design efficient materials based on porphyrins, capable to detect/recover PtNPs from leaching solution.

This novel approach relies on complexation phenomena between suitable porphyrins and platinum nanoparticles being both a facile method for the recovery of platinum from dilute solutions and a source of new platinum complexes.

Two amino-functionalized free-base porphyrins, an aliphatic one: 5,10,15,20-tetrakis(4-aminophenyl)porphyrin (TAPP) (Figure 1a) and an aromatic one: 5,10,15,20-tetrapyrrolyl-21H,23H-porphine (TPyP) (Figure 1b), were chosen to compare their distinctive abilities to recover platinum.

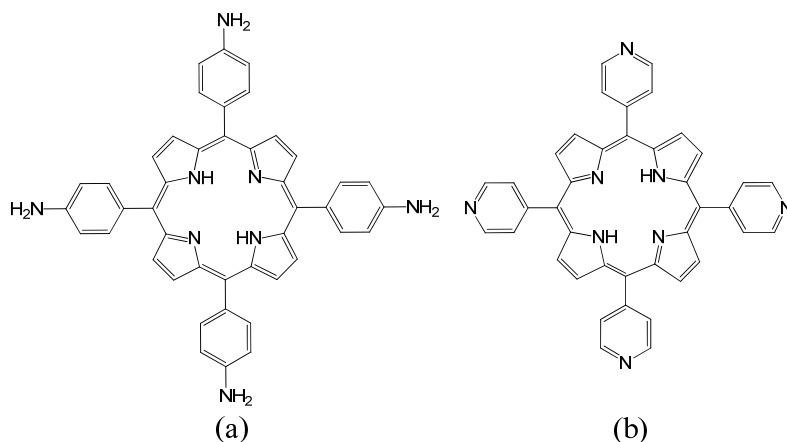


Figure 1. Structures of 5,10,15,20-tetrakis(4-aminophenyl)porphyrin (TAPP) (a) and 5,10,15,20-tetrapyrrolyl-21H,23H-porphine (TPyP) (b)

RESULTS AND DISCUSSION

1. UV-vis spectroscopy of Pt-colloid and amino-porphyrins in DMF and in acid solutions

The UV-vis spectra of Pt-colloid and amino-porphyrins both in DMF and in acid solutions are presented in Figure 2 A and B.

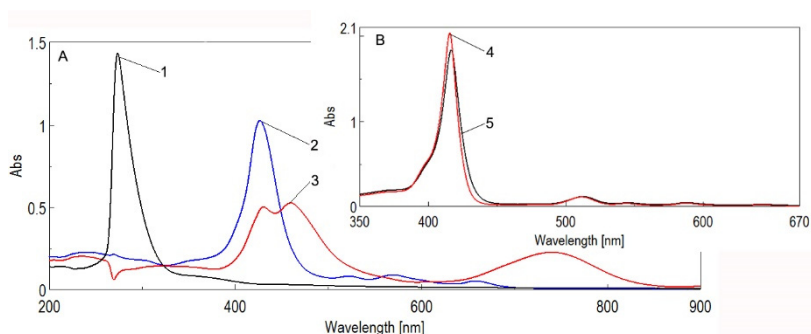


Figure 2. Overlapped UV-vis spectra of: Pt colloid in water (**A1**); **TAPP** in DMF ($c = 1.989 \times 10^{-5} \text{M}$) (**A2**); **TAPP** in acid environment ($\text{pH} = 2.5$) (**A3**); **TPyP** in DMF ($c = 8.834 \times 10^{-5} \text{M}$) (**B4**); **TPyP** in acid environment ($\text{pH} = 2.5$) (**B5**)

From Figure 2A-line 1, it can be observed that the maximum absorption peak for the platinum colloidal solution, located at $\lambda_{\text{max}} = 274 \text{ nm}$, (figure T line 1) does not belong to the visible region of the spectrum.

The TAPP porphyrin shows (Figure 2A-line 2), as expected, the intense Soret band at 426 nm accompanied by only three Q bands, located at: 522 nm, 569 nm and respectively 658 nm.

In the case of TAPP (Figure 2A-line 3), when reaching a $\text{pH} = 2.5$, after HCl 0.5 N solution was added, the splitting of the Soret band occurs due to the protonation of the two imino nitrogens from the inner structure of porphyrin. The deprotonation is accompanied by the disappearance of the Q2 and Q3 bands accompanied by both a significant hyperchromic effect and highly bathochromic shift of the Q1 band up to 740 nm. All these aspects are indicative for an J-type aggregation process (side-by side arrangement of molecules) that is investigated further by AFM. Regarding TPyP (Figure 2B-line 4), at the same $\text{pH} = 2.5$, only a shift of the Soret band from 416 nm to 418 nm can be noticed, that might be the sign for a beginning of J-type aggregation.

2. Platinum colloid detection

2.1. Uv-vis monitoring of the complex generation between TAPP and PtNPs in acidulated medium

The complex generation between TAPP and PtNPs in acid medium was continuously monitored by UV-vis spectroscopy (Figure 3).

By continuously adding of controlled amounts of PtNPs to the acidulated TAPP solution, a few complex phenomena took place. The first effect is the decrease in the intensity of the Soret band situated around 460 nm that is accompanied by a hypsochromic shift of around 5 nm.

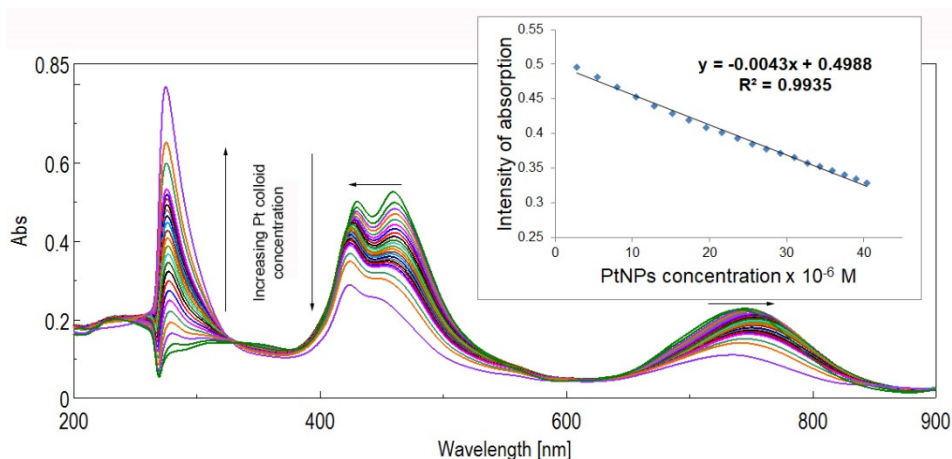


Figure 3. Overlapped UV-vis spectra monitoring the complex formation. In detail: linear dependence between the intensity of absorption of the hybrid Pt-TAPP read at 460 nm and PtNPs concentration

The same effect might be observed regarding the second Soret band initially located at 430 nm that is also blue shifted from 430 to 425 nm.

A clear isosbestic point, located around 325 nm, and another one at 630 nm, indicate the formation of PtNPs-porphyrin complex, so that these optical effects cannot be explained by simple dilution.

The absorption maximum corresponding to the Pt plasmon is also hypsochromically shifted, from 274 nm to 276 nm.

In the range of PtNPs concentrations from 2.776 to 40.457 x 10⁻⁶ M the dependence between the intensity of absorption of the plasmonic band read at 460 nm and the increasing concentration of PtNPs is linear, characterized by an excellent correlation coefficient of 99.35 % (Figure 3-detail).

2. 2. *Uv-vis monitoring of the complex generation between TPyP and PtNPs in acidulated medium*

The successive adding of platinum colloid to the TPyP acidulated solution in DMF ($c = 8.834 \times 10^{-5}$ M) leads to the formation of a complex nanomaterial, Pt-TPyP, evidenced by the presence of two isosbestic points, at 391 nm and 426 nm respectively, on both branches of the Soret band of the spectrum. A simple dilution phenomenon is excluded due to both the isosbestic points existence and because of the increasing in intensity of the Q bands (Figure 4 and A and B details).

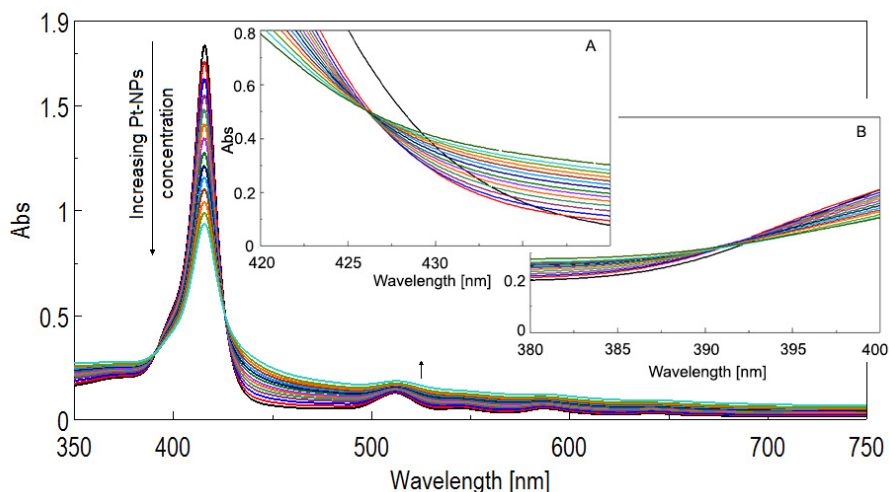


Figure 4. Overlapped UV-vis spectra after successive adding of Pt-NPs solution to acidulated TPyP and isosbestic points detail: isosbestic point at 426 nm (A) and isosbestic point at 391 nm (B)

The dependence between the intensity of absorption of the Soret band read at 416 nm and PtNPs concentration is linear with an excellent correlation coefficient of 99.57 % in the platinum concentration range: $8.07 \times 10^{-6} - 7.03 \times 10^{-5}$ M, as represented in Figure 5. These values are comparable to those detectable by TAPP porphyrin, proving that both porphyrins containing amino groups, either aliphatic or aromatic, are capable to form complexes with platinum nanoparticles.

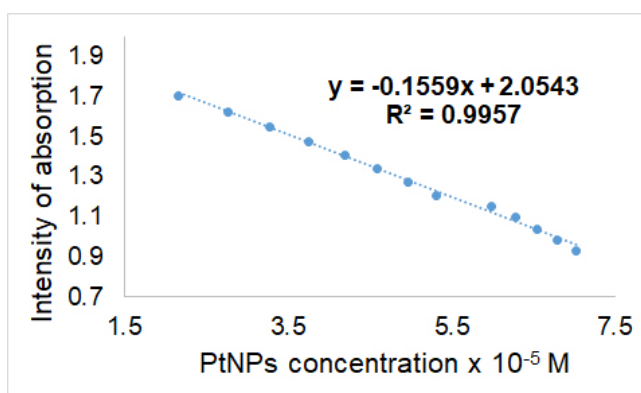
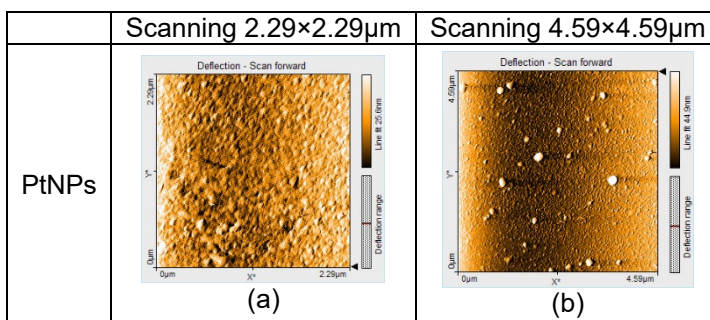


Figure 5. Linear dependence between the intensity of absorption of the Soret band read at 416 nm and PtNPs concentration

3. AFM investigation of the Pt colloid, bare porphyrins and hybrid nanomaterials

Table 2 (A, B, C) presents the main results from AFM investigation, regarding surface features, morphology and aggregation architectures. Table 2A reveals that the dimension of Pt-colloid ovoid-like particles is varying in the range of 65 - 80 nm (Table 1A, a and b) having the height distribution in the domain of 6 - 14 nm. In the sized image of 4.59 x 4.59 μm the formation of some large platinum spherical shaped aggregates around 220 nm can be noticed, as expected from an unstabilized colloid.

Table 1A. AFM images of PtNPs (a,b)



The microscopy analysis was performed for TAPP porphyrin both solely and in acid pH medium. TAPP deposited by drop-casting from DMF on silica plates presents equilateral triangular building-block units (Table 1B, c and d), with dimensions larger than those generated in acid medium (Table 2B, e, f), having the sizes around 165 nm. The larger image (4.59 \times 4.59 μm) puts into evidence besides the continuous covering of the surface with triangular architectures preserving the same orientation, a novel type of organization in bow-type wires, implying that both types of aggregation processes, an initial H-type aggregation followed by the J- type phenomenon, are occurring.

Acidulated TAPP deposited on silica plates (Table 1B, e and f) presents the same orientation of triangular-shaped aggregates having sizes around 135 nm. The height distribution is tighter, in the region from 2.2 to 5.3 nm. In the 3-D image of acidulated TAPP (Table 1B, g) it can be seen triangular prisms randomly covering the surface and having the heights of 12 nm. This aspect is a novelty, because the usual aggregation of porphyrins in acid media is in the pyramidal form [38].

Table 1B: AFM images of investigated compounds: TAPP (c, d); acidulated TAPP (e, f, g); TAPP-PtNPs hybrid (h, i)

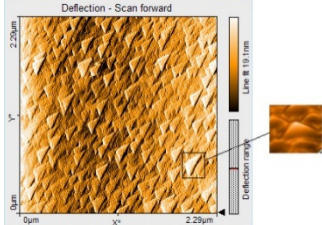
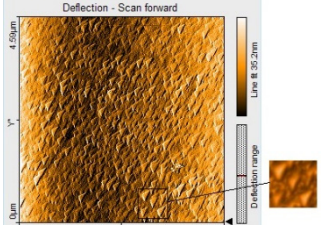
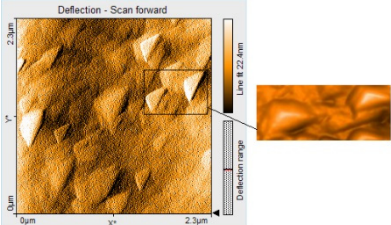
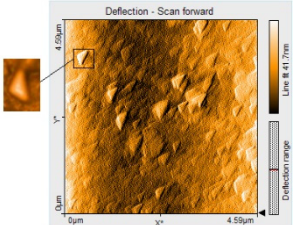
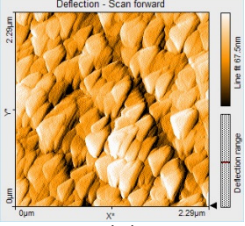
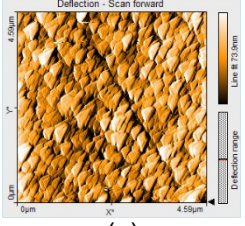
	Scanning 2.29×2.29µm	Scanning 4.59×4.59µm
TAPP	<p>(c)</p>	<p>(d)</p>
acidulated TAPP	<p>(e)-2D image</p> <p>(g)-3D image</p>	<p>(f)</p>
TAPP-PtNPs hybrid	<p>(h)</p>	<p>(i)</p>

Regarding the rugosity, a comparison between the porphyrin-base in DMF and in acidulated DMF-water medium reveals that the acid surfaces have a smaller rugosity (S_a varying from 2 nm to 4.6 nm) than those in DMF solution (S_a from 3 nm to 6.4 nm).

In the case of the hybrids obtained between porphyrin and Pt colloid (Table 1B, h and i), the height distribution is smaller and narrower and the sizes are varying from 5 to 8.3 nm. The hybrid nanomaterial has the whole structure reorganized showing smaller triangular particles with dimension of 35 nm. In conclusion, the generation of complex between the TAPP and the PtNPs in acid media gave rise to a very well-structured nanomaterial, characterized by a slightly higher rugosity than that of TAPP in different media, that is around 3.2 nm.

Regarding the pyridyl substituted derivative, TPyP, a roof type aggregation can be seen (Table 1C, j and k) at the interface DMF-air, generated by H- and J-type processes using as building blocks triangular isosceles with dimensions of 122nm and 204 nm, respectively and height distribution in the range of 4-10 nm.

Table 1C: AFM images of the investigated compounds: TPyP (j, k); acidulated TPyP (l, m); TPyP-PtNPs hybrid (n, o)

	Scanning 2.29×2.29µm	Scanning 4.59×4.59µm
TPyP	 <p>(j)</p>	 <p>(k)</p>
TPyP acidulated	 <p>(l)</p>	 <p>(m)</p>
TPyP-PtNPs hybrid	 <p>(n)</p>	 <p>(o)</p>

When the TPyP is deposited from DMF acid medium (Table 1C, l and m), the rugosity is increasing, this aspect being divergent with the behavior of TAPP.

In the 3-D images (Table 1C, l-detail), the architecture of the aggregates is a pyramidal one, that is another different aspect as compared to TAPP.

The hybrid micromaterial, TPyP-PtNPs (Table 1C, n and o) has the surface morphology constituted from equilateral triangles having dimensions of around 320 - 450 nm, that are amazingly organized as the bricks in a wall (generated by sandwich-type aggregation) and showing distinct rows (generated by J-type aggregation).

The height distribution is in this particular case larger, in the range of 22 - 70 nm.

The recovery of PtNPs

The recovery of PtNPs was performed as previously reported [34] by precipitating PtNPs from the two obtained hybrid materials using 1 N HCl solution (Figure 6A).

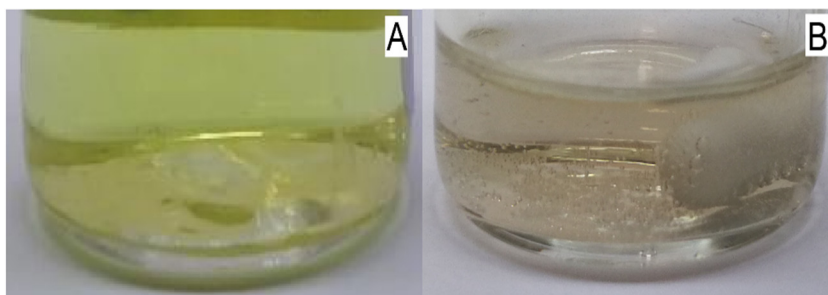


Figure 6. Reduction of the PtNPs-porphyrin complexes using 1N HCl (A) and NaBH₄ (B)

The recovery efficiency of these two aminoporphyrins was evaluated from the capacity of complexation and the results are promising: 602 mg Pt /g TAPP and 212 mg Pt /g TPyP, corresponding to approximately 3 mole PtNPs/ 1 mole TAPP and 1 mole PtNPs/ 1 mole TPyP. A plausible explanation might be that TAPP is capturing PtNPs in the inner part of the molecule and also between the -NH₂ functional groups (from 5,10 and 15, 20) but the TPyP creates coordinative bonds only in the center of the molecule.

CONCLUSIONS

The design of efficient materials based on different amino-substituted porphyrins, capable to detect or recover PtNPs from leaching solution was the main aim of this study.

This novel approach relies on complexation phenomena between suitable porphyrins and platinum nanoparticles being both a facile method for the recovery of platinum from dilute solutions and a source of new platinum complexes.

Two amino-functionalized free-base porphyrins, an aliphatic one: 5,10,15,20-tetrakis(4-aminophenyl)porphyrin (TAPP) and an aromatic one: 5,10,15,20-tetrapyridyl-21H,23H-porphine (TPyP) were chosen to compare their distinctive abilities to recover platinum. The platinum from the synthetic leaching solution containing $\text{H}_2\text{PtCl}_6 \cdot 6\text{H}_2\text{O}$ was transformed in colloidal Pt by reducing with NaBH_4 .

The complexation reactions were monitored by UV-vis spectroscopy and revealed that each of these porphyrins have the capacity to complex PtNPs in different detection domains ranging from 2.776 to 40.457×10^{-6} M in the case of TAPP, and in a larger range of 8.07×10^{-6} – 7.03×10^{-5} M in the case of TPyP. Excellent correlation coefficients of 99.35% and 99.57 respectively have been obtained in each case.

During complexation a nanomaterial based on TAPP and a micromaterial composed from TPyP both having as second partner PtNPs were obtained and thoroughly characterized by AFM. The aggregation phenomena that occurred for each amino-porphyrin in DMF, in their acidified solutions and in their hybrid materials, revealed that the TAPP-PtNPs hybrid is a nanomaterial, and the TPyP-PtNPs hybrid is a micromaterial. Both hybrid materials have as building block units TAPP or TPyP already aggregated in triangular geometries of different sizes (with two or all three sides equal), but always uniformly oriented.

The recovery efficiency of these two aminoporphyrins was evaluated from the capacity of complexation and the results are promising: 602 mg Pt /g TAPP and 212 mg Pt /g TPyP, corresponding to approximately 3 moles PtNPs/ 1 mole TAPP and 1 mole PtNPs/ 1 mole TPyP.

EXPERIMENTAL SECTION

Reagents

Hexachloroplatinic acid and trisodium citrate were purchased from Sigma-Aldrich (St. Louis, USA). Sodium borohydride was provided by Merck (Darmstadt, Germany) and doubly distilled water was used for all experiments.

The synthesis of TAPP was done in two steps involving the obtaining of 5,10,15,20-*meso* -tetrakis-(*p*-nitrophenyl) porphyrin, followed by the reduction of nitro-groups with $\text{SnCl}_2 \times 2\text{H}_2\text{O}$ [39].

The synthesis of TPyP was done in accordance with published results [40] starting from 4-pyridinecarboxaldehyde and pyrrole in propionic acid.

Synthesis of the platinum colloid

In order to check the viability of PtNPs complexation and its total recovery after the reduction of complexes, we used for the platinum colloid generation $\text{H}_2\text{PtCl}_6 \times 6\text{H}_2\text{O}$, thus creating an ideal situation. In real leaching solutions, a mixture of valuable metal ions, such as: Pt (in the form of $(\text{NH}_4)_2\text{PtCl}_6$), Pd and Rh are present, besides Ni and Mn ions that are not interfering.

So, the platinum colloid was synthesized after previously reported data [41], as follows: a solution was prepared from 0.01697 g (3.276×10^{-5} mole) of $\text{H}_2\text{PtCl}_6 \times 6\text{H}_2\text{O}$ dissolved in 77.9 mL distilled water with molar concentration of $c = 1.416 \times 10^{-4}$ M. To this solution 2 mL trisodium citrate with $c = 0.04$ M were added and stirred for 30 minutes at room temperature. After 30 minutes of vigorous stirring 0.409 mL NaBH_4 solution with concentration 0.05 M, was added dropwise. The mixture was stirred and allowed to react at ambient temperature for 1 h.

The solution color changed from yellowish to brownish yellow due to optical phenomena associated to the formation of nanometric particles [42].

Obtaining the TAPP-Pt-colloid complex

To a volume of 5 mL TAPP in DMF ($c = 1.808 \times 10^{-5}$ M) 0.1 mL portions of Pt colloid solution ($c = 1.416 \times 10^{-4}$ M) in water were added. The mixture was stirred for 30 seconds and then the UV-vis spectra were recorded and overlapped (as shown in Figure 3).

Obtaining the TPyP-Pt-colloid complex

The experiment was done in a similar way, changing only the concentration of TPyP solution in DMF ($c = 8.834 \times 10^{-5}$ M). The overlapped UV-vis spectra were registered (as shown in Figure 4).

Method for the recovery of PtNPs

The two obtained complexes PtNPs-TAPP and PtNPs-TPyP were subjected to a reduction reaction using 1N HCl and NaBH_4 solutions and it was clearly proven that the platinum nanoparticles were precipitated.

Apparatus

For recording UV-visible spectra a V-650 - JASCO spectrometer (Pfungstadt, Germany) having 1 cm wide quartz cuvettes was used. Atomic force microscopy (AFM) images were obtained on a Nanosurf®EasyScan 2 Advanced Research AFM microscope (Liestal, Switzerland). The samples were deposited on pure silica plates by drop casting from DMF solution.

ACKNOWLEDGMENTS

This research is funded by UEFISCDI, project ECOTECH-GMP 76 PCCDI/2018, belonging to PNIII-Future and Emerging Technologies and partially by Romanian Academy through Programme 3/2020 from Institute of Chemistry “Coriolan Dragulescu”.

REFERENCES

1. J. Kou; D. Dou; L. Yang; *Oncotarget*, **2017**, *8(46)*, 81591-81603.
2. J.S. Rebouças; B.R. James; *Inorg Chem.*, **2013**, *52(2)*, 1084–1098.
3. M.R. Civic; P.H. Dinolfo; *ACS Appl. Mater. Interfaces*, **2016**, *8(31)*, 20465–20473.
4. J. Barona-Castaño; C. Carmona-Vargas; T. Brocksom; K. de Oliveira; *Molecules*, **2016**, *21(3)*, 310.
5. G. Bottari; O. Trukhina; M. Ince; T. Torres; *Coord. Chem. Rev.*, **2012**, *256(21-22)*, 2453–2477.
6. X. Qian; L. Lu; Y.-Z. Zhu; H.-H. Gao; J.-Y. Zheng; *RSC Advances*, **2016**, *6(11)*, 9057–9065.
7. O. Rezazgui; G. Marchand; P. Trouillas; B. Siegler; S. Leroy-Lhez; *Chemistry Select*, **2018**, *3(39)*, 10959–10970.
8. X. Sun; G. Chen; J. Zhang; *Dyes Pigment.*, **2008**, *76(2)*, 499–501.
9. C. Liu; S.C. Sun; X.P. Zhu; G.F. Tu; J.Y. Zhang; *IOP Conf. Series: Materials Science and Engineering*, **2019**, *479*, 012058.
10. G.V. Fedorenko; L.P. Oleksenko; N.P. Maksymovych; I.P. Matushko; *Russ. J. Phys. Chem. A*, **2015**, *89(12)*, 2259–2262.
11. E. Fagadar-Cosma; I. Sebarchievici; A. Lascu; I. Creanga; A. Palade; M. Birdeanu; B. Taranu; G. Fagadar-Cosma; *J. Alloys Compd.*, **2016**, *686*, 896–904.
12. C.A. Mak; M.A. Pericas; E. Fagadar-Cosma; *Catal. Today*, **2018**, *306*, 268–275.
13. T.C. Johnstone; K. Suntharalingam; S.J. Lippard; *Chem. Rev.*, **2016**, *116(5)*, 3436–3486.
14. A.L. Stepanov; A.N. Golubev; S.I. Nikitin; Y.N. Osin; *Rev. Adv. Mater. Sci.*, **2014**, *38*, 160-175
15. A.S. Dehnavi; A. Raisi; A. Aroujalian; *Synth. React. Inorg. Met.-Org. Nano-Metal Chem.*, **2013**, *43(5)*, 543–551.
16. L. Dykman; A. Lyakhov; V.A. Bogatyrev; S. Shchyogolev; *November Colloid Journal*, **1998**, *60(6)*, 700-704.
17. A. Martinez-Abad; *Multifunctional and Nanoreinforced Polymers for Food Packaging*, **2011**, 347–367.

18. L. Kacenauskaite; J. Quinson; H. Schultz; J.J.K. Kirkensgaard; S. Kunz; T. Vosch; M. Arenz; *Chem Nano Mat*, **2016**, 3(2), 89–93.
19. J. Quinson; M. Inaba; S. Neumann; A.A. Swane; J. Bucher; S.B. Simonsen; L.T. Kuhn; J.J.K. Kirkensgaard; K.M.O. Jensen; M. Oezaslan; S. Kunz; M. Arenz; *ACS Catalysis*, **2018**, 8(7), 6627–6635.
20. T.M. Tolaymat; A.M. El Badawy; A. Genaidy; K.G. Scheckel; T.P. Luxton; M. Suidan; *Sci Total Environ.*, **2010**, 408(5), 999–1006.
21. L.S. Nair; C.T. Laurencin; *Prog. Polym. Sci.*, **2007**, 32(8-9), 762–798.
22. S. Kato; R. Hokama; H. Okayasu; Y. Saitoh; K. Iwai; N. Miwa; *JNN*, **2012**, 12(5), 4019–4027.
23. X. Wang; P. Sonström; D. Arndt; J. Stöver; V. Zielasek; H. Borchert; K. Thiel; K. Al-Shamery; M. Bäumer; *J. Catal.* **2011**, 278(1), 143–152.
24. D.A. Gregory; S.J. Ebbens; *Langmuir*, **2018**, 34(14), 4307–4313.
25. L. Zhang; Y. Lu; Y. Du; P. Yang; X. Wang; *J Porphyr Phthalocya*, **2010**, 14(06), 540–546.
26. E.R. Clark; D.M. Kurtz; *Inorg. Chem.*, **2017**, 56(8), 4584–4593.
27. K. Ladomenou; M. Natali; E. Iengo; G. Charalampidis; F. Scandola; A.G. Coutsolelos; *Coord. Chem. Rev.*, **2015**, 304-305, 38–54.
28. H.-J. Hong; H. Yu; M. Park; H.S. Jeong; *Carbohydr. Polym.*, **2019**, 210, 167–174.
29. D.J. Garole; B.C. Choudhary; D. Paul; A.U. Borse; *Environ Sci Pollut Res*, **2018**, 25(11), 10911–10925.
30. A.K. Mosai; L. Chimuka; E.M. Cukrowska; I.A. Kotzé; H. Tutu; *Miner. Eng.*, **2019**, 131, 304–312.
31. H. Malekian; M. Salehi; D. Biria; *Waste Manag.*, **2019**, 85, 264–271.
32. T. Suoranta; O. Zugazua; M. Niemelä; P. Perämäki; *Hydrometallurgy*, **2015**, 154, 56–62.
33. D. Anghel, I. Frațilescu, A. Lascu; *New trends and strategies in the chemistry of advanced materials with relevance in biological systems, technique and environmental protection*, **2019**, 6-7.
34. A. Lascu; Proceedings of the 25th International Symposium on Analytical and Environmental Problems, **2019**, 18-22.
35. M.S. Safarzadeh; M. Horton; A.D. Van Rythoven; *Min Proc Ext Met Rev*, **2017**, 39(1), 1–17.
36. Y. Ding; H. Zheng; J. Li; S. Zhang; B. Liu; C. Ekberg; Z. Jian; *Metals*, **2019**, 9(3), 354.
37. A.N. Nikoloski; K.L. Ang; D. Li; *Hydrometallurgy*, **2015**, 152, 20–32.
38. E. Fagadar-Cosma; G. Fagadar-Cosma; M. Vasile; C. Enache; *Curr. Org. Chem.*, **2012**, 16, 931–941
39. A. Bettelheim; B.A. White; S.A. Raybuck; R.W. Murray; *Inorg. Chem.*, **1987**, 26, 1009-1017.
40. E. Fagadar-Cosma; C. Enache; I. Armeanu; G. Fagadar-Cosma; *Dig. J. Nanomater. Bios.*, **2007**, 2, 175 – 183.
41. G.W. Wu; S.B. He; H.P. Peng; H.H. Deng; A.L. Liu; X.H. Lin; X.H. Xia; W. Chen; *Anal. Chem.*, **2014**, 86(21), 10955–10960.
42. B. Escobar Morales; S.A. Gamboa; U. Pal; R. Guardián; D. Acosta; C. Magaña; X. Mathew; *Int. J. Hydrog. Energy*, **2010**, 35(9), 4215–4221.